Particulate Science and Technology, 20: 341–354, 2002

0272-6351/02 $12.00 + .00
DOI: 10.1080/02726350290058164

Taylor & Francis
Taylor & Francis Group

Evaluation of Free-Fall Particle CT Images Using State Transition Matrix

MASAHIRO TAKEI
MITSUAKI OCHI

Department of Mechanical Engineering
College of Science and Technology, Nihon University
Tokyo, Japan

YOSHIFURU SAITO

Hosei University
Tokyo, Japan

KIYOSHI HORII

Shirayuri College
Tokyo, Japan

Spatial particle density distribution images in a pipe cross section have been evaluated by means of state transition matrix, which is a parameter indicating the dominant particle density transition patterns among time series images consisting of CT 2-D space and 1-D time. State transition characterizes the transition patterns for positions in a cross section as monotonous transitions, sudden transitions, and extreme value transitions. In a simulation, the real part of the state transition matrix is negative and the imaginary part is zero in the case of monotonous transition. The real part is positive and the imaginary part is zero in the case of extreme value transition. The imaginary part is nonzero in the case of sudden transition. In free-fall particles in a vertical pipe, high, sudden, and extreme value transitions do not occur because the particle flow rate at this position is low, and therefore the probability of collision among particles is also low. High, sudden, and extreme value transitions occur near the pipe center when the particle flow rate is high, because the probability of collision among particles is high.

Keywords: state transition matrix, capacitance CT, free-fall particles, image processing

Introduction

Movements of particles, powders, and granules have been scrutinized in an effort to attain high performance operation in chemical engineering facilities such as air transportation equipment and circulating fluidized beds. For example, particle density distribution in particle-laden turbulent channel flow was measured by the

Address correspondence to Masahiro Takei, Department of Mechanical Engineering, College of Science and Technology, Nihon University, Tokyo, Japan. E-mail: takei@mech.cst.nihon-u.ac.jp

laser sheet method (Fessler et al., 1994), and the distribution in channel flow was calculated by large eddy simulation (Wang & Squires, 1996). Moreover, total particle density at a pipe center line of free-fall particles in a vertical standpipe was measured by a laser method (Peng & Herrmann, 1995). These studies reveal that nonuniformity of particle density occurs in the flow direction when the particle flow rate is high. However, these studies have been conducted with respect to the pipe axial direction rather than the pipe cross section. Meanwhile, a cluster formation of particles in a circulating fluidized bed, which is an extreme case of nonuniformity, has been visualized with respect to both the pipe axial direction and the pipe cross section by the laser sheet method (Horio & Kuroki, 1994). However, cluster formation in the cross section was visualized from an inclined viewpoint and was not estimated quantitatively.

Against this background, the process tomography method has been developed in order to visualize particle behavior in multiphase flow in pipe cross section noninvasively and quantitatively (Huang et al., 1989). This capacitance tómography CT, method was applied to gas-solid flow in a pipeline in order to visualize the particle density distribution in the pipe cross section in time series (Dyakowski et al., 1999). Takei et al. (2002) have decomposed the CT images with an image processing technique of wavelet multi-resolution to point out nonuniform distribution of the particle density not only in the flow direction but also in the cross section. However, combination of CT and image processing raises a new issue: how to evaluate nonuniformity of the time transitional particles from the time discretized CT images by means of a mathematical method.

In other fields related to fluid engineering, the state transition matrix method is quite often used as a method to evaluate a time transitional relationship between time responses. For instance, the state transition matrix method is introduced in order to evaluate the vibration response between coolant flow and a fluid structure of a nuclear reactor (Kuzelka, 1982). This method is used also to calculate the deposition process of sputtered neutral particles in a chemical reaction chamber (Parker et al., 1995). Generally, the state transition matrix has been used in such one-dimensional time transitional relationships, but it has not been applied to three-dimensional image fields consisting of two-dimensional space (x and y) by one-dimensional time.

In the present study, the state transition matrix is defined in order to evaluate simple imitated particle density images among discretized CT images and to discuss characteristics. Moreover, the state transition matrix method is applied to CT images of free-fall particles in a vertical pipe for evaluating the time transitional particle density distribution.

Theory of State Transition Matrix to CT Images

A standard cross section in Figure 1 depicts free-fall particle movement in a coordinate system of a pipe. The particle density changes at a position between a standard cross section at time t and a cross section at $t + \Delta t$ by two factors space interactions and time transition. The governing Equation is assumed to be a Helmholtz-type differential Equation, which expresses particle movement in the cross section for a given time t:

$$\nabla^2 U + \alpha \frac{\partial U}{\partial t} + \beta \frac{\partial^2 U}{\partial t^2} = -\rho \tag{1}$$

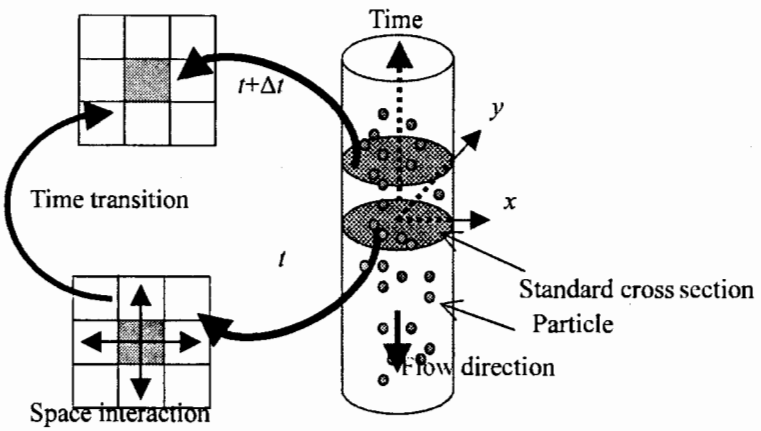

Figure 1. Coordinate system in a pipe and particle density factors.

where U is the particle density distribution with 2-D space x and y, and time t in the cross section, α and β are coefficients with dimension $[t/m^2]$ and $[t^2/m^2]$, respectively. For $\alpha = 0$, Equation (1) is called a wave equation, and for $\beta = 0$, Equation (1) is called a diffusion equation. This study assumes that the particle diffusion is dominant rather than the particle wave in free-fall particles in a pipe, which expresses $\beta = 0$. In Equation (1), ρ is source density, which is dependent on the space and time. The first term in Equation (1) indicates spatial dispersion, and the second term indicates time transition of particle density.

After $\nabla^2 U$ is discretized by a discretization method, Equation (1) is rewritten as:

$$\mathbf{C}\boldsymbol{U}_t + \gamma \frac{d}{dt}\boldsymbol{U}_t = \boldsymbol{K} \tag{2}$$

$\boldsymbol{U}_t$ is a $1 \times n^2$ vector when both image space resolution in x and y directions are n. $\mathbf{C}$ is a discretization coefficient of an $n^2 \times n^2$ matrix, which is composed of coefficients of U. In the case of nine-point finite difference method and zero Dirichlet boundary condition, the relationship between continuous and discrete systems is:

$$\frac{\partial^2 U_{i,j}}{\partial x^2} + \frac{\partial^2 U_{i,j}}{\partial y^2} \approx \frac{1}{6\Delta h}[U_{i-1,j-1} + U_{i-1,j+1} + 4U_{i-1,j} + U_{i+1,j+1} + U_{i+1,j-1} + 4U_{i,j+1} + 4U_{i,j-1} - 20U_{i,j}]$$

where i and j are the x and y position in the cross section. In Equation (2), γ and $\boldsymbol{K}$ are:

$$\gamma = \Delta h^2 \alpha, \quad \boldsymbol{K} = -\Delta h^2 \boldsymbol{\rho}$$

where Δh is a distance between the discrete grids. $\boldsymbol{K}$ is dependent on $\boldsymbol{\rho}$, which is source density $1 \times n^2$vector. Based on Equation (2), the continuous particle density U in Equation (1) becomes the discrete particle density $\boldsymbol{U}_t$, which is dependent on time only. Multiplying Equation (2) by γ^{-1} yields

$$\frac{d}{dt}U_t = -\mathbf{A}U_t + \boldsymbol{F} \tag{3}$$

where $\mathbf{A} = \gamma^{-1}\mathbf{C}$ and $\boldsymbol{F} = \gamma^{-1}\boldsymbol{K}$. In Equation (3), $\mathbf{A}$ is the state transition value matrix governing the particle density transition, which is an $n^2 \times n^2$ matrix, and $\boldsymbol{F}$ is a $1 \times n^2$ input vector.

Because Equation (3) cannot be resolved directly, mode coordinates are considered. The mode matrix consisting of the eigenvector of $\mathbf{A}$ is replaced by $\boldsymbol{Z}$, and $\boldsymbol{U}_t$ is rewritten using linear coupling between the element of $\mathbf{Z}$ and the element of vector $\boldsymbol{Y}$:

$$\boldsymbol{U}_t = \mathbf{Z}\boldsymbol{Y} \tag{4}$$

where $\mathbf{Z} = [z_1, z_2, z_3, \ldots, z_{n\times n}]$, z_1 is a transpose vector of the first eigen vector of $\mathbf{A}$. After Equation (4) is substituted into Equation (3), it is rewritten as:

$$\frac{d}{dt}\boldsymbol{Y} = -\mathbf{\Lambda}_\mathbf{p}\boldsymbol{Y} + \mathbf{Z}^\mathbf{T}\boldsymbol{F} \tag{5}$$

where $\mathbf{Z}^{-1} = \mathbf{Z}^\mathbf{T}$ because $\mathbf{Z}$ is an orthonormal matrix, and $\mathbf{\Lambda}_\mathbf{p} = \mathbf{Z}^\mathbf{T}\mathbf{A}\mathbf{Z}$. $\mathbf{\Lambda}_p$ is the transition matrix of the real physical system indicating particle density transition, which is a square matrix with diagonal elements of the eigenvalues of $\mathbf{A}$. The solution vector of the modal Equation (5) is:

$$\boldsymbol{Y}_t = \mathbf{\Lambda}_\mathbf{p}^{-1}\mathbf{Z}^\mathbf{T}\boldsymbol{F} + e^{-\mathbf{\Lambda}_\mathbf{p}t}(\mathbf{Y}_0 - \mathbf{\Lambda}_\mathbf{p}^{-1}\mathbf{Z}^T\boldsymbol{F}) \tag{6}$$

where Y_0 is the initial vector. When the vector from the input vector $\boldsymbol{F}$ is replaced with Y_f, Equation (6) is rewritten as:

$$\boldsymbol{Y}_t = \boldsymbol{Y}_f + e^{-\mathbf{\Lambda}_\mathbf{p}t}(\boldsymbol{Y}_0 - \boldsymbol{Y}_f) \tag{7}$$

Because $\mathbf{Z}e^{-\mathbf{\Lambda}_\mathbf{p}t} = e^{-\mathbf{\Lambda}_\mathbf{p}t}\mathbf{Z}$, when $\mathbf{Z}$ multiplies Equation (7) from the left side,

$$\boldsymbol{U}_t = \boldsymbol{U}_f + e^{-\mathbf{\Lambda}_\mathbf{P}t}[\boldsymbol{U}_0 - \boldsymbol{U}_f] \tag{8}$$

is obtained. Equation (8) means the density distribution $\boldsymbol{U}_t$ at an arbitrary time t is expressed by the first particle density distribution $\boldsymbol{U}_0$ and the final particle density distribution $\boldsymbol{U}_f$.

In Equation (8), in the case of $t = 0$, the intermediate density distribution $\boldsymbol{U}_t$ is equal to the initial density distribution $\boldsymbol{U}_0$ in the case of $t \to \infty$, the intermediate density distribution $\boldsymbol{U}_t$ is equal to the final density distribution $\boldsymbol{U}_f$. When Equation (8) is applied among three discretized CT images, the following relation holds:

$$\boldsymbol{U}_{i+1} = \boldsymbol{U}_{i+2} + e^{-\mathbf{\Lambda}\Delta t}[\boldsymbol{U}_i - \boldsymbol{U}_{i+2}] \tag{9}$$

where i is the frame number of CT images and Δt is the time resolution of CT images. The state transition matrix in the image system $\mathbf{\Lambda}$ indicates the transition quantities

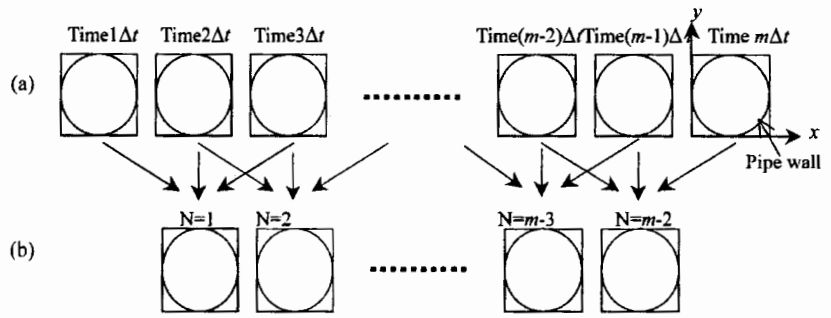

Figure 2. CT image and state transition matrix $\mathbf{\Lambda}$. (a) CT image m frames; (b) state transition matrix $\mathbf{\Lambda}$ $m-2$ frames.

among three images. On the basis of Equation (9), the state transition matrix $\mathbf{\Lambda}$ is rewritten as:

$$\mathbf{\Lambda} = \frac{-1}{\Delta t} \ln \left[\frac{\boldsymbol{U}_{i+1} - \boldsymbol{U}_{i+2}}{\boldsymbol{U}_i - \boldsymbol{U}_{i+2}} \right] \tag{10}$$

where $\mathbf{\Lambda}$ is an $n^2 \times n^2$ diagonal matrix of eigenvalues λ; however, the element position is replaced with column and row order to easily visualize the transition as an image:

$$\mathbf{\Lambda} = \begin{bmatrix} \lambda_1 & & & \\ & \lambda_2 & & 0 \\ & & \ddots & \\ & 0 & & \lambda_{n\times n-1} \\ & & & & \lambda_{n\times n} \end{bmatrix} \Rightarrow \mathbf{\Lambda} = \begin{bmatrix} \lambda_1 & \lambda_1 & \cdots & \lambda_1 & \lambda_n \\ \lambda_{n+1} & & \cdots & & \\ & & \cdots & & \\ & & \cdots & & \\ & 1 & \cdots & \lambda_{n\times n-1} & \lambda_{n\times n} \end{bmatrix}$$

Figure 2 shows the relationship between the time series of CT images and $\mathbf{\Lambda}$. On the basis of Equation (10), $\mathbf{\Lambda}$ of $(m-2)$ frames are obtained as shown in Figure 2(b) when the discretized images have m frames as shown in Figure 2(a). When $\mathbf{\Lambda}$ is calculated, the particle movement characteristic among three images is extracted as linear or nonlinear.

Simulation

The fundamental characteristics of $\mathbf{\Lambda}$ should be confirmed by use of an imitational one-pixel image. As shown in Table 1, the density transition among three images from U_i, U_{i+1}, and U_{i+2} and has nine simple patterns. Moreover, except for the constant pattern in Table 1, the transition patterns are classified into three patterns as shown in Figure 3. These are: a monotonous transition, a sudden transition, and an extreme value transition. In particular, pattern numbers (2) through (7) in Table 1 are classified into two patterns: the sudden transition shown in Figure 3 (b), and the extreme value transition shown in Figure 3(c). A sudden transition state is said to occur when the intensity of the final image U_{i+2} is located between the first image $\boldsymbol{U}_i$ and the intermediate image U_{i+1}. Similarly, an extreme value transition occurs when

Table 1
Time Transition among Three Images

No.	Image	Transition direction	Image	Transition direction	Image
(1)	U_i	UP[a]	U_{i+1}	UP	U_{i+2}
(2)		UP		DOWN[b]	
(3)		UP		CONSTANT[c]	
(4)		CONSTANT		UP	
(5)		CONSTANT		DOWN	
(6)		CONSTANT		CONSTANT	
(7)		DOWN		UP	
(8)		DOWN		DOWN	
(9)		DOWN		CONSTANT	

[a]Increase of transition quantity between images.
[b]Decrease of transition quantity between images.
[c]Constant transition quantity between images.

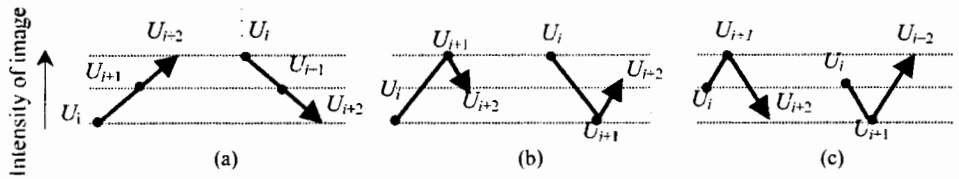

Figure 3. Examples of density transition. (a) monotonous transition; (b) sudden transition; (c) extreme value transition.

the intensity of the first image U_i falls between the intermediate image U_{i+1} and the final image U_{i+2}. The simple density transition functions, i.e., a monotonous function, a noncontinuous function, and a decrement function, are substituted into Equation (10) for discussing the relationship between the transition pattern and Λ.

First, a monotonous function is considered. Particle density that shows monotonous transition is assumed to follow

$$U_t = e^{-t} \tag{11}$$

at one-image pixel as shown in Figure 4. The horizontal axis represents time t, and the vertical axis represents image intensity U_t, which is assumed to be the density value. Substituting Equation (11) into Equation (10) leads to the state transition matrix Λ shown in Figure 5. According to Figure 5, the real part of Λ has a continuous negative value and the imaginary part of Λ is zero.

Second, the noncontinuous function is considered. Particle density that shows noncontinuous transition is assumed to follow

$$U_t = e^{-|t-20|} \tag{12}$$

at one-image pixel as shown in Figure 6. Substituting Equation (12) into Equation (10) leads to the state transition matrix Λ shown in Figure 7. According to Figure 7,

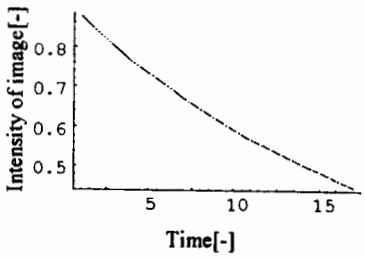

Figure 4. Imitated monotonous function at one-image pixel.

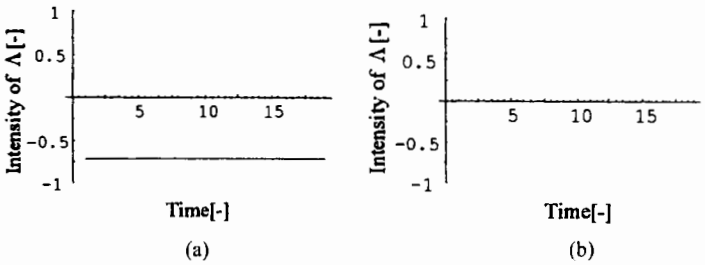

Figure 5. State transition matrix **Λ**. (a) Real part of **Λ**; (b) imaginary part of **Λ**.

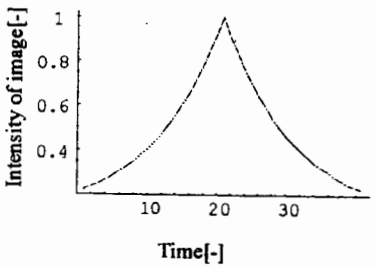

Figure 6. Imitated noncontinuous function at one-image pixel.

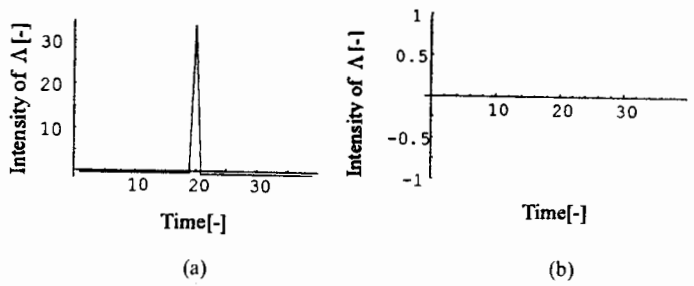

Figure 7. State transition matrix **Λ**. (a) Real part of **Λ**; (b) imaginary part of **Λ**.

the real part of Λ has a peak at the noncontinuous point, and the imaginary part is zero.

Third, the decremental function is considered in a similar manner. Particle density, which shows decrement transition, is assumed to follow

$$U_t = \cos(\beta t)e^{-\alpha t} \tag{13}$$

at one-image pixel as shown in Figure 8, where α and β are constants. Substituting Equation (13) into Equation (10) leads to the state transition matrix Λ shown in Figure 9. According to Figure 9, the real part and the imaginary part have peaks at the extreme point.

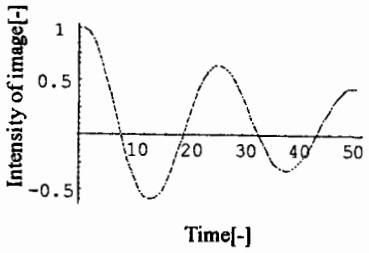

Figure 8. Imitated decrement function at one-image pixel.

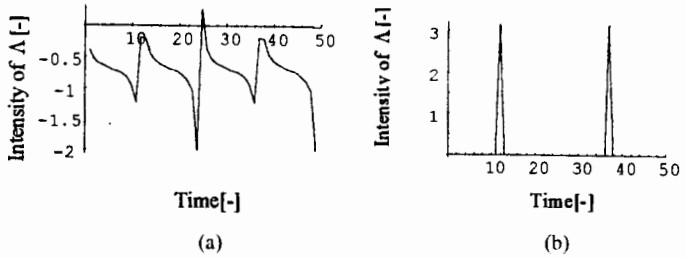

Figure 9. State transition matrix Λ. (a) Real part of Λ; (b) imaginary part of Λ.

Table 2
Relationship Between Density Transition Pattern and Λ

Density transition pattern	State transition matrix Λ			
	Real part		Imaginary part	
	Positive	Negative	Positive	Negative
Monotonous transition	×[a]	[b]	0 (zero)	
Extreme value transition	0	×		
Sudden transition	0	0	0	×

[a]Value does not exist.
[b]Value exists.

On the basis of the above-mentioned simulation, the fundamental relationship between the density transition pattern and Λ is clarified as shown in Table 2. When the density pattern is monotonous transition, the real part of Λ is negative and the imaginary part of Λ is zero. Similarly, when the density pattern is extreme value transition, the real part of Λ is positive and the imaginary part of Λ is zero. Moreover, when the density pattern is sudden transition the imaginary part of Λ is nonzero. In other words, as shown in Table 2, the real part of Λ and the imaginary part of Λ determine the nature of density transition.

Experiments

Principle of Capacitance CT

Free-fall particle density distribution images were obtained in a vertical pipe by a CT sensor, depicted in Figures 10 (a) and (b) (Yang, 1996). Insulation materials separate the 12 electrodes within the sensor. The relationship between capacitance and permittivity in the static-electro field is expressed by:

$$C_{i,j} = -\frac{\varepsilon_0}{V_c} \oint_{r \subseteq \Gamma_j} \varepsilon(\mathbf{r}) \nabla V_i(\mathbf{r}) \cdot d\mathbf{r} \tag{14}$$

where i is the standard electrode number, which ranges from 1 to 11; j is the reference electrode number, which ranges from $i+1$ to 12; $C_{i,j}$ is the capacitance between the standard electrode i and the reference electrode j; ε_0 is the vacuum permittivity of air; $\varepsilon(\mathbf{r})$ is the permittivity distribution on the cross section; $\mathbf{r}$ is a position vector on the cross section; V_c is the voltage supplied to the ith electrode; Γ_j is the area affected by the electric line of force; and $V_i(\mathbf{r})$ is the potential distribution on the cross section between the ith and jth electrodes. Since $V_i(\mathbf{r})$ is unknown in Equation (14), the Laplace equation

$$\nabla \cdot [\varepsilon(\mathbf{r}) \nabla V(\mathbf{r})] = 0 \tag{15}$$

is assumed in the cross section. $V(\mathbf{r})$ is obtained from the discretized Equation (15).

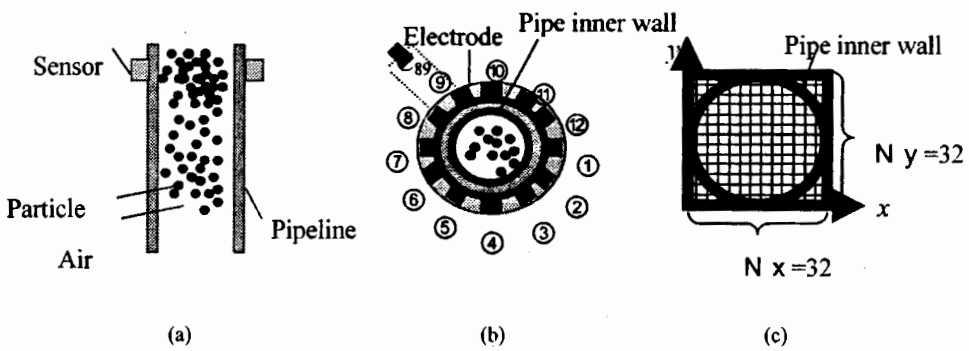

Figure 10. Overview of capacitance CT and its spatial resolution. (a) Frontal view; (b) cross-sectional-view; (c) spatial resolution.

The matrix expression in Equation (14) showing the relationship between the capacitance vector $\boldsymbol{C}$ and the permittivity distributions vector $\boldsymbol{E}$ is

$$\boldsymbol{C} = \mathbf{S}_e \boldsymbol{E} \tag{16}$$

where $\mathbf{S}_e$ is the sensitivity map matrix. In other words, the capacitance CT can be used to obtain the permittivity distribution of the particles $\boldsymbol{E}$ in the cross section from both the known sensitivity map matrix $\mathbf{S}_e$ and the measured capacitance matrix $\boldsymbol{C}$. In the case where the pipeline cross section has 12 electrodes and $32 \times 32 = 1024$ pixels, as in the spatial resolution shown in Figure 10 (c), the sensitivity map $\mathbf{S}_e$ is a 66×1024 matrix in Equation (16), the capacitance matrix $\boldsymbol{C}$ expresses a 66×1 matrix, and the permittivity distribution matrix $\boldsymbol{E}$ is a 1024×1 matrix. The mathematical method used to obtain the permittivity matrix $\boldsymbol{E}$ from both the capacitance matrix $\boldsymbol{C}$ and the sensitivity map matrix $\mathbf{S}_e$ is an ill-posed inverse problem, because the inverse matrix $\mathbf{S}_e^{-1}$ does not exist. In this study, the Newton-Raphson method (Isaksen, 1996) is used to obtain the permittivity matrix $\boldsymbol{E}$.

Experimental Equipment, Conditions, and Results

Figure 11 shows the experimental equipment, which is composed of a hopper for supplying particles, a vertical pipe, the CT sensor, and a receiver. The pipe is 2 m long and has an inside diameter of 50 mm. Polyethylene pellets are dropped in free-fall from the hopper at three flow rates, $Q_1 = 9.82 \times 10^{-5}\,\mathrm{m^3/s}$, $Q_2 = 2.55 \times 10^{-4}\,\mathrm{m^3/s}$, and $Q_3 = 6.04 \times 10^{-4}\,\mathrm{m^3/s}$. Mean particle diameter is 3.26 mm. The

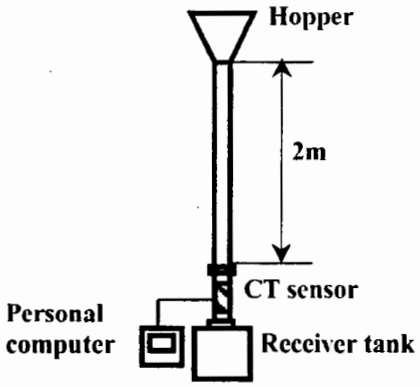

Figure 11. Experimental equipment.

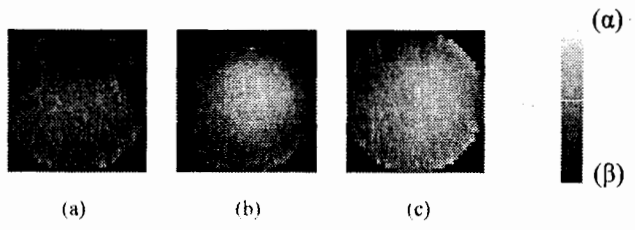

Figure 12. Visualized time-mean CT images. (a) Q_1: (α)0.07, (β)−0.04; (b) Q_2: (α)0.21, (β)−0.08; (c) Q_3: (α)0.15, (β)−0.03.

resulting images consist of 171 frames obtained at 100 Hz interval; i.e., Δt is 10 milliseconds. Figures 12 (a), (b), and (c) show the time-mean images visualized by the CT sensor at the three particle volume flow rates. The white region indicates high density, and the black region indicates low density. The image values are normalized in each image; the conditions differ in maximum and minimum values. According to the time-mean images, the near center position has a high value, and the value gradually decreases toward the pipe wall. Figure 13 shows the spatial mean value of the particle density of each image. The density fluctuation DF is calculated by:

$$DF = \sum_{t} \sum_{y} \sum_{x} \sqrt{[E_{xyt} - \overline{E_t}]^2}$$

where $\overline{E_t}$ is a space-mean density value at time t CT image. According to the figure, the spatial mean value increases; moreover, the spatial mean value fluctuates to a greater extent as the particle flow rate increases. Figures 14 (a) and (b) show the time-mean values for each image on the one-pixel line of x axis and one-pixel line of y axis. According this figure, the particle in the case of Q_1 and Q_2 concentrate in the

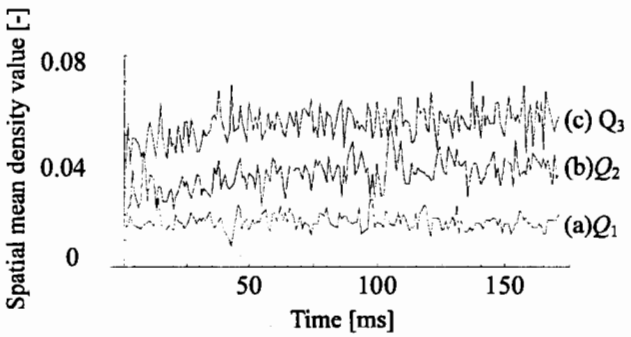

Figure 13. Spatial mean values for each image. (a) Time and space mean density = 0.017[−], density fluctuation = 0.007[−]; (b) Time and space mean density = 0.035[−], density fluctuation = 0.013[−]; (c) Time and space mean density = 0.054[−], density fluctuation = 0.018[−].

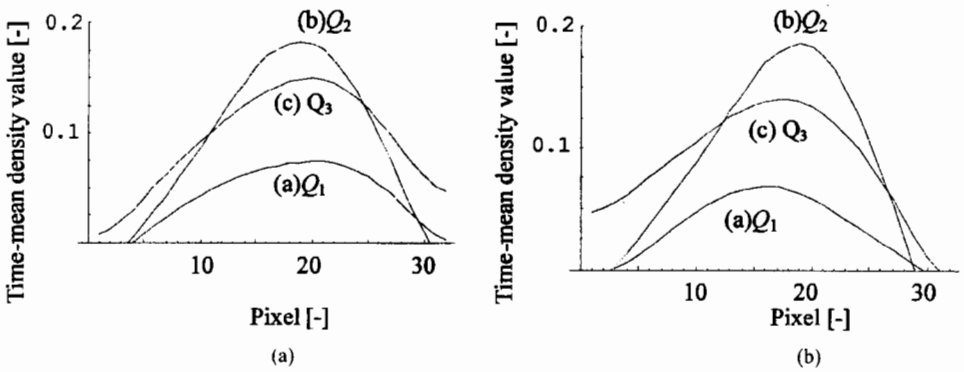

Figure 14. Time-mean values for each image. (a) One-pixel line of x axis; (b) one-pixel line of y axis.

pipe center; however, the particle distribution in the case of Q_3 is broader and the particle disperse to the pipe wall.

Image Processing and Discussion

Image Processing Method

In order to clarify the density transition in the pipe cross section, a transition pattern map among three discrete images at a given time was produced. The process to produce the map is as follows: first, three images $\boldsymbol{E}$ in time order are substituted into $\boldsymbol{U}$ in Equation (10) in order to obtain the transition matrix $\boldsymbol{\Lambda}$. Second, on the basis of the value pattern of $\boldsymbol{\Lambda}$, the dominant density transition pattern; namely, monotonous transition, sudden transition, or extreme value transition, is judged from Table 2. Third, the transition pattern map in the pipe cross section is produced by binarizing the density transition pattern; namely, when sudden transition is extracted, the pixel of the sudden transition is replaced with 1.0, which is indicated by white, and the pixel of the other transition or nontransition is replaced with 0.0. When extreme value transition is extracted, the pixel of the extreme transition is replaced with 1.0, and the pixel of the other transition or nontransition is replaced with 0.0. Finally, the process from the first step to the third step is repeated for all images in time sequence. As a result, the positions where the kinds of transition patterns occur in the cross section are qualitatively visualized.

Image Processing Results and Discussion

Figure 15 shows an example of the transition pattern map among $99\Delta t$, $100\Delta t$, and $101\Delta t$ for three values of particle flow rates. This figure is the trinarization map of the transition patterns. Figure 16 is the time-mean binarizing transition pattern map obtained from the total time. (*)-1 is the sudden transition, and (*)-2 is the extreme value transition. The white region indicates high intensity of the transition, and the black region indicates low intensity of the transition. According to Figure 16 (a)-1, in the case of low particle flow rate Q_1, the high sudden transition (white region) slightly occurs near the pipe wall and the pipe center. As can be seen from Figure 16(a)-2, the extreme value transition also slightly occurs near the pipe wall. According to Figures 16(b)-1 and -2, in the case of intermediate particle flow rate Q_2, the intensity of the sudden transition (white region) relatively increases near the pipe center; however, the intensity of sudden and extreme value transitions near the pipe wall are nearly the same as the Q_1 case. Based on Figures 16(c)-1 and -2, in the case of high particle flow rate Q_3, the sudden transition and the extreme value transition

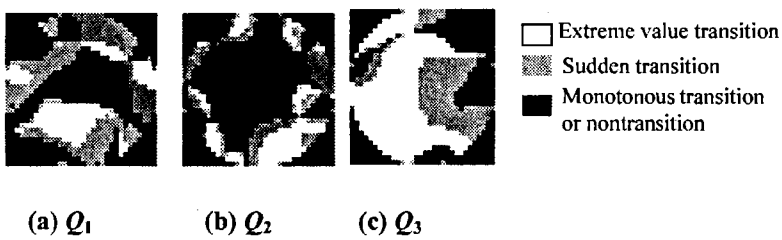

(a) Q_1 (b) Q_2 (c) Q_3

Figure 15. Examples of transition pattern maps.

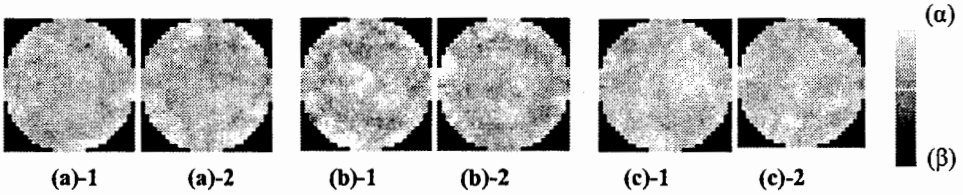

Figure 16. Time-mean transition pattern maps. ( )-1 Sudden transition; ( )-2 extreme value transition. (a)Q_1: (α)0.10, (β)−0.22; (b)Q_2: (α)0.14, (β)−0.28; (c)Q_3: (α)0.12, (β)−0.22.

strongly occur on the whole. According to Figure 12, the time-mean particle density tends to be dense near the pipe center irrespective of the particle flow rate. However, the transitional process of the particle density in the cross section is strongly dependent on particle flow rate. In the case of Q_1 in Figure 13, the fluctuation of the particle density is low: 0.007. The extreme value transition does not occur frequently near the pipe center, because the collision frequency among particles is low near the center. Also, according to Figure 14, because the particles tend not to be located near the pipe wall, the intensity of the sudden and extreme value transitions is small. On the other hand, in the case of Q_3 in Figure 13, the fluctuation of the particle density is high: 0.018. Moreover, the particles are dispersed in the whole cross section as shown in Figure 14. The sudden transition and extreme value transition occur near the pipe center and the pipe wall, because the particles move in various directions by collision between particles and collision between particles and the pipe wall. In the case of intermediate particle flow rate Q_2, the pattern shows characteristics falling between those of the low particle flow rate pattern and those of the high particle flow rate pattern.

In free-falling particles in a pipeline, so-called inhomogeneous particle density is reported. In the case of large particle size, such as that used in this study, the dominant factor for inhomogeneous particle density becomes particle collision rather than turbulence. Peng and Herrmann (1995) calculated the particle density in a cross section of a standpipe by the lattice gas automation (LGA) method on the condition that particles fall freely from the upper part of the pipe. According to the paper, when particle density is low (in the case of particle injection rate), the power spectrum density (P.S.D.) maintains the same value. This means the particle density is homogeneous, because the probability of collision between particles is low. However, the P.S.D. decreases with increasing time frequency when the particle density is high (in the case of particle injection rate). This means that the particle density becomes inhomogeneous because the particles collide with one another and with the wall. The aforementioned discussion in this image processing results shows qualitative agreement with the previously reported research results under similar experimental conditions.

Conclusions

The state transition matrix $\mathbf{\Lambda}$ has been defined from the Helmholtz-type differential Equation to apply to evaluation of the particle transitional process. As a preliminary study, $\mathbf{\Lambda}$ is applied to the imitated particle density in a simple one-image pixel in order to confirm the relationship between $\mathbf{\Lambda}$ values and transition patterns among three images, namely, monotonous transition, sudden transition, and extreme value

transition. Moreover, Λ is applied to free-fall particle density distribution images visualized by a CT sensor in order to discuss the particle transition patterns. The following results are obtained:

(1) In the case of monotonous transition, the real part of Λ is negative and the imaginary part of Λ is zero. In the case of sudden transition, the real part of Λ is nonzero and the imaginary part of Λ is positive. In the case of extreme value transition, the real part of Λ is positive and the imaginary part of Λ is zero.

(2) Sudden transition and extreme value transition does not occur frequently when the particle flow rate is low, because the probability of collision among particles is relatively low. On the other hand, the transitions occur near the pipe center when the particle flow rate is high, because the probability of collision among particles is high.

References

Dyakowski, T., S. P. Luke, K. L. Ostrowski, & R. A. Williams. 1999. On-line monitoring of dense phase flow using real time dielectric imaging. *Powder Technol.* 104: 287–295.

Fessler, J. R., J. D. Kulick, & J. K. Eaton. 1994. Preferential concentration of heavy particles in a turbulent channel flow. *Phys. Fluids.* 6(11): 3742–3749.

Horio, M., & H. Kuroki. 1994. Three-dimensional flow visualization of dilute dispersed solids in bubbling and circulating fluidized beds. *Chem. Eng. Sci.* 49(15): 2413–2421.

Huang, S. M., A. B. Plaskowski, C. G. Xie, & M. S. Beck. 1989. Tomographic imaging of two-component flow using capacitance sensors. *J. Phys. E: Sci. Instrum.* 22: 173–177.

Isaksen, O. 1996. A review of reconstruction techniques for capacitance tomography. *Measur. Sci. Technol.* 7(3): 325–337.

Kuzelka, V. 1982. A solution of the vibrational response reactor components to random exciting forces due to coolant flow. *Nucl. Eng. and Des.* 72(2): 189–196.

Parker, G. J., W. N. G. Hitchon, & D. J. Koch. 1995. Transport of sputtered neutral particles. *Phys. Rev. E.* 51(4): 3694–3703.

Takei, M., H. Li, M. Ochi, Y. Saito, & K. Horii. 2002. Feature extraction of particle density in a pipeline with tomography and wavelets. *Int. J. Appl. Electromagn. Mech.*, 11: (in press).

Peng, G. & H. J. Herrmann. 1995. Density waves and 1/f density fluctuations in granular flow. *Phys. Rev. E.* 51(3): 1745–1756.

Wang, Q., & K. D. Squires. 1996. Large eddy simulation of particle-laden turbulent channel flow. *Phys. Fluids.* 8(5): 1207–1223.

Yang, W. Q., 1996. Hardware design of electrical capacitance tomography systems. *Measur. Sci. & Technol.* 7(3): 225–232.